ELSEVIER

Nuclear Instruments and Methods in Physics Research B 187 (2002) 285–301

NIM B
Beam Interactions with Materials & Atoms

www.elsevier.com/locate/nimb

Energy loss of relativistic heavy ions in matter

B.A. Weaver*, A.J. Westphal

Space Sciences Laboratory, University of California, Berkeley, CA 94720-7450, USA

Received 28 August 2001; received in revised form 9 October 2001

Abstract

We have investigated the theory of energy loss of charged particles in matter due to ionization of the medium, integrating the work of other authors over several decades. We describe the most important corrections to standard energy-loss formulae. We compare our calculations to an improved measurement of the range of 1 A GeV U ions and to other codes and tabulations. We show that calculations based on the theory of ionization energy loss are at least as accurate as tabulations extrapolated from empirical data for the stopping of uranium ions in matter. We have made available the computer code resulting from our investigations. © 2002 Elsevier Science B.V. All rights reserved.

PACS: 34.50.Bw
Keywords: Energy loss; Stopping power; Heavy ions

1. Introduction

The theory of energy loss has been developed in many parts, since there are many phenomena which must be included in a complete description of energy loss. Since these phenomena are described in many different publications over many decades, we have collected here the mathematical expressions of these phenomena with modern and uniform notation. As we will show, good agreement with experimental results and with tables of extrapolated empirical ranges can be obtained from calculations based on the most relevant portions of the theory of energy loss. In the course of this investigation we have developed a new, open-source code based on this theory which has applications in cosmic-ray instrumentation, among other applications.

2. Theory of energy loss

2.1. The overall form

The overall form of the energy-loss formula can be obtained from classical arguments [1]. In SI units, that formula is

$$-\frac{\mathrm{d}E}{\mathrm{d}x} = \frac{Z_1^2 e^4 n_\mathrm{e}}{4\pi\epsilon_0^2 m_\mathrm{e} v^2} L. \tag{1}$$

Here, Z_1 is the charge of the projectile, and m_e and n_e are the electron mass and number density,

* Corresponding author. Tel.: + 1-510-642-9733; fax: + 1-510-643-7629.
E-mail address: weaver@curium.ssl.berkeley.edu (B.A. Weaver).
URL: http://ultraman.ssl.berkeley.edu/~weaver/.

0168-583X/02/$ - see front matter
PII: S0168-583X(01)01143-0

respectively. The minus sign on the left-hand side is simply a reminder that the formula gives the energy *lost* by the particle and is therefore an overall negative quantity. The factor L is the stopping logarithm, defined classically by

$$L = \ln \frac{b_{\max}}{b_{\min}}, \tag{2}$$

where $b_{\max}$ and $b_{\min}$ are the maximum and minimum impact parameters, respectively. Typically we use units of A MeV g^{-1} cm^2, ("A MeV" is to be read "MeV per nucleon") in which case this becomes

$$-\frac{dE}{dx'} = 4\pi N_A m_e c^2 r_e^2 \frac{Z_1^2 Z_2}{A_1 A_2} \frac{1}{\beta^2} L, \tag{3}$$

where we have made the replacement $x \to x' = \rho x$. Here, Z_2 and A_2 are the atomic number and atomic mass, respectively, of the target material, A_1 is the atomic mass of the projectile, N_A is Avogadro's number, and $r_e = e^2/4\pi\epsilon_0 m_e c^2$ is the classical electron radius.

The devil, they say, is in the details. In this case, the detail is the stopping logarithm L. Following Lindhard and Sørensen [2], we define

$$L_0 = \ln\left(\frac{2m_e c^2 \beta^2 \gamma^2}{I}\right) - \beta^2 - \frac{\delta}{2}. \tag{4}$$

This is the form of L derived originally from quantum perturbation theory – the first two terms are typically called the Bethe result. The third term is the density effect (see Section 2.3). The notation, $-\delta/2$, for the magnitude of the density effect, is historical. Here, I is the effective ionization potential of the target material. Although there are theoretical means to determine I, the experimentalist should regard it as an empirical parameter. Throughout what follows, we will refer to the form $L = L_0$ as the "Bethe" form of dE/dx.

For an accurate calculation, further corrections of the form $L = L_0 + \Delta L$ are required. It will be useful here to define the quantity

$$\eta \equiv \frac{\alpha Z_1}{\beta}, \tag{5}$$

where $\alpha = e^2/4\pi\epsilon_0\hbar c$ is the usual fine-structure constant. It is most desirable to find formulae for ΔL which will be valid for all values of η, since for heavy ions we cannot assume $\alpha Z_1 \ll 1$.

2.2. Composite materials

Often we must deal with target materials which are not pure elements. Glasses, plastics, and alloys are all common targets. For these, energy loss may be calculated by the so-called Bragg rule: The total energy loss is the weighted sum of the energy lost due to each element in the target [3]. Since it is the number of electrons which is important in stopping, it is most sensible to start with the expression (Eq. (1)) which contains the electron number density explicitly.

The most important application of the Bragg sum rule is the derivation of the effective mean ionization potential for composite materials:

$$Z_2 \ln I = \sum_i f_i Z_i \ln I_i, \tag{6}$$

where f_i is the mole fraction of the ith element. It has been recommended [4] that the value $I_i = 1.13 I_i^E$ be used in Eq. (6), where I_i^E is the value of I used for the pure element.

2.3. The density effect

Although we have included the density effect as part of the "Bethe" form of the total energy loss, it is worthwhile to discuss it separately since it is important to the discussion of relativistic rise. Unlike many high-energy corrections, the density effect can actually be at least qualitatively derived in classical electrodynamics. Such a derivation may be found in Jackson [1]. In dense media, the field which perturbs electrons far from the projectile track is modified by the dielectric polarization of the atoms between the distant electron and the projectile. The magnitude of the density effect was originally calculated by Fermi [5] and extended by Sternheimer and Peierls [6].

At high energies, the density effect correction has the form

$$-\frac{\delta}{2} = -\ln(\beta\gamma) + \ln\frac{I}{\hbar\omega_p} + \frac{1}{2}, \tag{7}$$

where ω_p is the plasma frequency of the medium. The density effect reduces the relativistic rise from $\sim\ln\gamma^2$ to $\sim\ln\gamma$ and substitutes the plasma frequency for the mean ionization potential. At

somewhat lower energies, the density effect is more complicated, but typically a parametric fit to the full density effect can be obtained. This parameterization was developed by Sternheimer and Peierls [6]. They define $X \equiv \log_{10}(\beta\gamma)$, and the density effect takes the form

$$-\frac{\delta}{2} = -\frac{\delta_{\text{high}}}{2} - \frac{a}{2}[X_1 - X]^m \quad (X_0 < X < X_1), \tag{8}$$

where X_0, X_1, a, and m are parameters which depend on the medium, and δ_{high} is obtained from Eq. (7). Typically, $X_0 \approx 0.1$, $X_1 \approx 3$, $a \approx 0.1$ and $m \approx 3$. In addition, there is a small low-energy density effect for conductors,

$$-\frac{\delta}{2} = -\frac{1}{2}\delta(X_0)10^{2(X-X_0)} \quad (X \leqslant X_0), \tag{9}$$

with the additional parameter $\delta(X_0) \approx 0.1$. For insulators, $\delta = 0$ for $X \leqslant X_0$. The most recent available tabulations of these density effect parameters may be found in [7]. Recent advances in computing power have made this parameterization essentially obsolete except for historical purposes. The density effect may now be computed by direct tabular interpolation for a single medium or by computing the complete density effect a priori [8].

2.4. The Bloch correction

This correction was derived by Bloch [9] in an investigation of the similarities and differences between classical and quantum-mechanical range-energy calculations. The full story can be found in Ahlen [10]. This correction may be placed in the form

$$\Delta L_{\text{Bloch}} = \psi(1) - \text{Re}\,\psi(1 + i\eta), \tag{10}$$

where

$$\psi(z) \equiv \frac{d}{dz}\ln\Gamma(z). \tag{11}$$

The numerical value of $\psi(1) = -0.5772157\ldots \equiv -\gamma_E$ is the negative of Euler's constant.

Although there are robust and highly accurate algorithms for computing values of the Gamma function (Appendix A), it is somewhat simpler to implement the Bloch correction as a sum, which can take two forms,

$$\begin{aligned}\Delta L_{\text{Bloch}} &= \sum_{l=1}^{\infty}\left[\frac{l}{l^2+\eta^2} - \frac{1}{l}\right] \\ &= -\eta^2\sum_{l=1}^{\infty}\left[\frac{1}{l}\frac{1}{l^2+\eta^2}\right].\end{aligned} \tag{12}$$

These are, of course, exactly equivalent. The second form of Eq. (12) suggests a common approximation to the Bloch correction. If η is small, the sum can be approximated by $\zeta(3) = 1.202057\ldots$, and thus we find a form frequently encountered,

$$\Delta L_{\text{Bloch}} \simeq -1.202\eta^2 \quad (\eta \ll 1). \tag{13}$$

2.5. The Mott correction

Corrections to energy loss of order higher than Z^2 at high energies first became apparent a few decades ago [11,12]. The origin of these higher order corrections is simply the Dirac equation which is, after all, the correct theory of the electron; the Mott cross-section is most appropriate for discussing the scattering of electrons off of highly charged nuclei. Ahlen [13] calculated a correction to energy loss using a parameterization of the Mott cross-section derived by Doggett and Spencer [14] and Curr [15]. Another derivation of the Mott correction is given in [16], but both forms contain minor typos. Here we give the form recommended by Ahlen [10],

$$\begin{aligned}\Delta L_{\text{Mott}} &= \frac{1}{2}\left\{\eta\beta^2\left[1.725 + \left(0.52 - 2\sin\frac{\theta_0}{2}\right)\pi\cos\chi\right]\right. \\ &\quad + \eta^2\beta^2(3.246 - 0.451\beta^2) \\ &\quad + \eta^3\beta^3\left(1.552\beta + \frac{0.987}{\beta}\right) \\ &\quad + \eta^4\beta^4\left(4.569 - 0.494\beta^2 - \frac{2.696}{\beta^2}\right) \\ &\quad \left. + \eta^5\beta^5\left(1.254\beta + \frac{0.222}{\beta} - \frac{1.170}{\beta^3}\right)\right\}.\end{aligned} \tag{14}$$

The parameter θ_0 is the same as in the Ahlen correction described in Section 2.6. Also

$$\cos\chi = \text{Re}\left[\frac{\Gamma\left(\frac{1}{2} - i\eta\right)\Gamma(1 + i\eta)}{\Gamma\left(\frac{1}{2} + i\eta\right)\Gamma(1 - i\eta)}\right]. \tag{15}$$

This can be placed in a somewhat more tractable form. Recognizing that $\Gamma(z^*) = [\Gamma(z)]^*$, Eq. (15) reduces to

$$\chi = 2\left[\arg\Gamma\left(\frac{1}{2} - \mathrm{i}\eta\right) + \arg\Gamma(1 + \mathrm{i}\eta)\right]. \tag{16}$$

An algorithm for computing the argument of the complex Gamma function is given in Appendix A. Finally, let us note that by rearranging the factors of η and β the term may be put in a form more tractable to calculation,

$$\begin{aligned}\Delta L_{\mathrm{Mott}} = \frac{1}{2}\eta\beta^2\Bigg\{&\left[1.725 + \left(0.52 - 2\sin\frac{\theta_0}{2}\right)\pi\cos\chi\right] \\ &+ \eta(3.246 - 0.451\beta^2) \\ &+ \eta^2(0.987 + 1.552\beta^2) \\ &+ \eta^3\left[-2.696 + \beta^2(4.569 - 0.494\beta^2)\right] \\ &+ \eta^4\left[-1.170 + \beta^2(0.222 + 1.254\beta^2)\right]\Bigg\}.\end{aligned} \tag{17}$$

It is recommended [13] that the Mott correction not be used for $Z_1/\beta > 100$, since the Mott correction becomes very large and negative at low energies, resulting in not only an incorrect but also an unphysical form for the energy loss.

2.6. The relativistic Bloch correction

It has been experimentally demonstrated that the Bloch correction is inadequate in regimes of both high charge and high energy [17]. An additional relativistic correction to the Bloch correction is necessary. This was first calculated by Ahlen [16]. Unfortunately, the original paper is not very accessible to the programmer who may wish to implement his formulae. Furthermore, it contains two free parameters which are not present in more sophisticated theories. Nevertheless, for historical reasons and comparisons with previous calculations, it is necessary to understand the form of this correction.

The overall form of what we will call the Ahlen correction is

$$\begin{aligned}\Delta L_{\mathrm{Ahlen}} = \frac{\pi}{2}\beta^2\eta\frac{\pi\eta\mathrm{e}^{\pi\eta}}{\sinh\pi\eta}&[(4\eta\ln 2)\mathrm{Re}\,L_1 \\ &+ (\pi\eta - 1)\mathrm{Im}\,L_1 + 2\eta\,\mathrm{Re}\,L_2],\end{aligned} \tag{18}$$

where

$$\begin{aligned}L_1 &= -\theta_0\frac{\mathrm{i}}{1 + \mathrm{i}2\eta}\left(\frac{\theta_0}{2}\right)^{\mathrm{i}2\eta} + \mathrm{i}\left(\frac{\alpha}{\beta\gamma\lambda}\right)^{1+\mathrm{i}2\eta}\frac{\mathrm{e}^{\mathrm{i}2\sigma}}{1 + \mathrm{i}2\eta} \\ &= -\frac{\mathrm{i}}{1 + \mathrm{i}2\eta}\left[2\left(\frac{\theta_0}{2}\right)^{1+\mathrm{i}2\eta} - \left(\frac{\alpha}{\beta\gamma\lambda}\right)^{1+\mathrm{i}2\eta}\mathrm{e}^{\mathrm{i}2\sigma}\right]\end{aligned} \tag{19}$$

and

$$\begin{aligned}L_2 &= -\theta_0\frac{\mathrm{i}}{1 + \mathrm{i}2\eta}\left(\frac{\theta_0}{2}\right)^{\mathrm{i}2\eta}\left(\ln\frac{\theta_0}{2} - \frac{1}{1 + \mathrm{i}2\eta}\right) \\ &\quad - \mathrm{i}\left(\frac{\alpha}{\beta\gamma\lambda}\right)^{1+\mathrm{i}2\eta}\frac{\mathrm{e}^{\mathrm{i}2\sigma}}{1 + \mathrm{i}2\eta}\left(\ln\frac{4\beta\gamma\lambda}{\alpha} + \gamma_{\mathrm{E}} - 1 + \frac{1}{1 + \mathrm{i}2\eta}\right) \\ &= -\frac{\mathrm{i}}{1 + \mathrm{i}2\eta}\left[2\left(\frac{\theta_0}{2}\right)^{1+\mathrm{i}2\eta}\left(\ln\frac{\theta_0}{2} - \frac{1}{1 + \mathrm{i}2\eta}\right)\right. \\ &\quad \left. + \left(\frac{\alpha}{\beta\gamma\lambda}\right)^{1+\mathrm{i}2\eta}\mathrm{e}^{\mathrm{i}2\sigma}\left(\ln\frac{4\beta\gamma\lambda}{\alpha} + \gamma_{\mathrm{E}} - 1 + \frac{1}{1 + \mathrm{i}2\eta}\right)\right].\end{aligned} \tag{20}$$

In both expressions

$$\sigma = \arg\Gamma(1 + \mathrm{i}\eta). \tag{21}$$

The two free parameters are θ_0 and λ. The first arises from considerations of Mott scattering, and can be thought of as an angular cut-off above which transverse momentum components may be neglected in the electron momentum. The parameter $\lambda = b_1/a_0$ represents the choice of close versus distant collision regimes, relative to the Bohr radius. These parameters are not completely independent since it is assumed $1/(k_0 b_1) \ll \theta_0 \ll 1$, where k_0 is the electron wave number in the center-of-mass frame of the problem. Ahlen [16] recommends $\theta_0 = 0.1$ and $\lambda = 1.0$. An energy-dependent form for θ_0 is given in [18]

$$\theta_0 = \sqrt{\frac{\alpha}{\beta\gamma\lambda}}, \tag{22}$$

that is, the geometric mean between $\alpha/\beta\gamma\lambda$ and 1.

Extracting the real and imaginary parts of these expressions is laborious. To evaluate these terms, first we define

$$\phi_1 = 2\eta \ln\frac{\theta_0}{2} \tag{23}$$

and

$$\phi_2 = 2\sigma + 2\eta \ln\frac{\alpha}{\beta\gamma\lambda}. \tag{24}$$

Then the desired real and imaginary parts can be expressed as

$$\mathrm{Re}\,L_1 = \frac{-\theta_0(2\eta\cos\phi_1 - \sin\phi_1) + \frac{\alpha}{\beta\gamma\lambda}(2\eta\cos\phi_2 - \sin\phi_2)}{1+4\eta^2} \tag{25}$$

and

$$\mathrm{Im}\,L_1 = \frac{-\theta_0(2\ \eta\sin\phi_1 + \cos\phi_1) + \frac{\alpha}{\beta\gamma\lambda}(2\eta\sin\phi_2 + \cos\phi_2)}{1+4\eta^2}. \tag{26}$$

The third term, $\mathrm{Re}\,L_2$, is

$$\begin{aligned}\mathrm{Re}\,L_2 = \Bigg\{ &-\theta_0\Bigg[\Bigg(\ln\frac{\theta_0}{2} - \frac{1}{1+4\eta^2}\Bigg)(2\eta\cos\phi_1 - \sin\phi_1) - \frac{2\eta}{1+4\eta^2}(2\eta\sin\phi_1 + \cos\phi_1)\Bigg] \\ &- \frac{\alpha}{\beta\gamma\lambda}\Bigg[\Bigg(\ln\frac{4\beta\gamma\lambda}{\alpha} + \gamma_{\mathrm{E}} - 1 + \frac{1}{1+4\eta^2}\Bigg)(2\eta\cos\phi_2 - \sin\phi_2) \\ &+ \frac{2\eta}{1+4\eta^2}(2\eta\sin\phi_2 + \cos\phi_2)\Bigg]\Bigg\}\frac{1}{1+4\eta^2}.\end{aligned} \tag{27}$$

As one might imagine, there are numerous avenues for algebraic errors to enter here, especially during the process of translating these formulae into computer code. In fact, the coder may find it more worthwhile to implement complex arithmetic so that the complex expressions (19) and (20) may be written directly into the code. While this does not reduce the complexity of the calculation, it dramatically increases the readability, resulting in fewer errors.

The Bloch, Mott and Ahlen corrections form what we will call hereinafter the BMA group both because of their common thread of development and the necessity for all three to be included together for precision calculations.

2.7. The Lindhard–Sørensen correction

The Lindhard–Sørensen (LS) correction, ΔL_{LS}, replaces the BMA group. In their paper Lindhard and Sørensen [2] show that the low-energy limit of the LS correction is *exactly* the Bloch correction. Furthermore, by using exact solutions to the Dirac equation, the LS correction automatically incorporates Mott scattering and is relativistically correct. (This definition of the LS correction differs from that of [19], where the Bloch and Mott corrections are still considered as separate.) The LS correction is given by

$$\Delta L_{\mathrm{LS}} = \sum_{k=-\infty\,(k\neq 0)}^{\infty}\left[\frac{|k|}{\eta^2}\frac{k-1}{2k-1}\sin^2(\delta_k - \delta_{k-1}) - \frac{1}{2|k|}\right] + \frac{1}{\eta^2}\sum_{k=1}^{\infty}\left[\frac{k}{4k^2-1}\sin^2(\delta_k - \delta_{-k})\right] + \frac{\beta^2}{2}, \tag{28}$$

where

$$\delta_k = \xi_k - \arg\Gamma(s_k + 1 + \mathrm{i}\eta) + \frac{\pi}{2}(l - s_k), \tag{29}$$

and with

$$\begin{aligned} s_k &= \sqrt{k^2 - (\alpha Z_1)^2}, \\ \mathrm{e}^{\mathrm{i}2\xi_k} &= \frac{k - \mathrm{i}\eta/\gamma}{s_k - \mathrm{i}\eta}, \\ l &= \begin{cases} k & (k>0), \\ -k-1 & (k<0). \end{cases}\end{aligned} \tag{30}$$

The quantity δ_k is a relativistic Coulomb phase shift and the summation over k is simply a

summation over a parameterization of the angular momentum quantum numbers (including spin). It is possible to show that

$$\tan(\delta_k - \delta_{-k}) = -\frac{\eta}{\gamma k}, \tag{31}$$

so that the second term of Eq. (28) becomes

$$\sum_{k=1}^{\infty} \frac{k}{4k^2-1} \frac{1}{\gamma^2 k^2 + \eta^2}. \tag{32}$$

When we take the difference in phase shifts we find

$$\begin{aligned}\delta_k - \delta_{k-1} = {} & \frac{1}{2}\arctan\frac{\eta(s_{k-1}-s_k)}{s_k s_{k-1}+\eta^2} \\ & + \frac{1}{2}\arctan\frac{\eta/\gamma}{k(k-1)+(\eta/\gamma)^2} \\ & - \arg\Gamma(s_k+1+\mathrm{i}\eta) \\ & + \arg\Gamma(s_{k-1}+1+\mathrm{i}\eta) \\ & - \frac{\pi}{2}\left(s_k - s_{k-1} - \frac{k}{|k|}\right).\end{aligned} \tag{33}$$

For ease of computation, it is simple to combine the summation terms in Eq. (28) into a single sum over positive k. Accordingly, we have

$$\begin{aligned}\Delta L_{\mathrm{LS}} = \sum_{k=1}^{\infty} \Bigg[& \frac{k}{\eta^2}\frac{k-1}{2k-1}\sin^2(\delta_k - \delta_{k-1}) \\ & + \frac{k}{\eta^2}\frac{k+1}{2k+1}\sin^2(\delta_{-k} - \delta_{-k-1}) \\ & + \frac{k}{4k^2-1}\frac{1}{\gamma^2k^2+\eta^2} - \frac{1}{k}\Bigg] + \frac{\beta^2}{2}.\end{aligned} \tag{34}$$

In this form, ΔL_{LS} converges roughly as k^{-3}. Note however, that some special care is required for the $k = 1$ term only. The phase shift δ_0 enters in the first summed term of Eq. (34) and because of the definition of s_k, it will be a complex number. Fortunately, the factor in front of $\sin^2(\delta_1 - \delta_0)$ is zero. Thus, it is recommended that for $k = 1$ only, the first term should be set to zero identically, rather than trying to force the computation of δ_0. A smoother evaluation of ΔL_{LS} will also be obtained if the correction is evaluated up to a particular value of k, rather than up to some fractional precision.

2.8. The finite nuclear size correction

In their paper Lindhard and Sørensen [2] also derive a correction due to the finite size of atomic nuclei. This is possible because exact solutions to the Dirac equation exist for any spherically symmetric potential [20,21]. We take the nuclear radius to be $R = 1.18A^{1/3}$ fm, and the dimensionless nuclear radius to be the ordinary radius divided by the electron Compton wavelength, $R' = Rm_e c/\hbar = 0.003056A^{1/3}$. The effect of finite nuclear size appears as a modification to the Coulomb phase shifts, Eq. (29). In this way, we can continue to use the summation in Eq. (28), but with new phase shifts given by

$$\begin{aligned}\delta_k &= \arg\left[\mathrm{e}^{\mathrm{i}\delta_k^{\mathrm{r}}} + H_k \mathrm{e}^{\mathrm{i}\delta_k^{\mathrm{s}}}\right] \\ &= \arctan\frac{\sin\delta_k^{\mathrm{r}} + H_k\sin\delta_k^{\mathrm{s}}}{\cos\delta_k^{\mathrm{r}} + H_k\cos\delta_k^{\mathrm{s}}},\end{aligned} \tag{35}$$

where δ_k^{r} is given by Eq. (29) δ_k^{s} can be obtained from Eq. (29) by the replacement $s_k \to -s_k$ throughout (including ξ_k). Note however, that we must sum Eq. (28) and not Eq. (34), since the relationship in Eq. (31) no longer applies. The phase shift δ_k^{s} is the phase shift arising from the solution to the Dirac equation in the Coulomb potential which is singular at the origin. The real number H_k, which provides the connection between the interior uniform sphere potential and the exterior Coulomb potential, is very complicated to evaluate in comparison to δ_k^{r}. First, the main expression for H_k is

$$H_k = \frac{F^{\mathrm{r}}/G^{\mathrm{r}} - F^{\mathrm{i}}/G^{\mathrm{i}}}{F^{\mathrm{i}}/G^{\mathrm{i}} - F^{\mathrm{s}}/G^{\mathrm{s}}}\frac{G^{\mathrm{r}}}{G^{\mathrm{s}}}. \tag{36}$$

The four ratios – $F^{\mathrm{r}}/G^{\mathrm{r}}$, $F^{\mathrm{i}}/G^{\mathrm{i}}$, $F^{\mathrm{s}}/G^{\mathrm{s}}$ and $G^{\mathrm{r}}/G^{\mathrm{s}}$ – are themselves complicated expressions which we define below. First we consider the ratio

$$\frac{F^{\mathrm{r}}}{G^{\mathrm{r}}} = \sqrt{\frac{\gamma-1}{\gamma+1}}\frac{\mathrm{Re}\,\Lambda^{\mathrm{r}}}{\mathrm{Im}\,\Lambda^{\mathrm{r}}}. \tag{37}$$

We define the quantity

$$\begin{aligned}\Lambda^{\mathrm{r}} \equiv {} & \exp[\mathrm{i}(\xi_k^{\mathrm{r}} - \beta\gamma R')] \\ & \times M(s_k+1+\mathrm{i}\eta, 2s_k+1, \mathrm{i}2\beta\gamma R'),\end{aligned} \tag{38}$$

where M is the confluent hypergeometric function (Appendix B). In addition, the ratio $F^{\mathrm{s}}/G^{\mathrm{s}}$ may be

obtained from Λ^{s} by the substitution $s_k \to -s_k$ throughout Eq. (38). The ratio $G^{\mathrm{r}}/G^{\mathrm{s}}$ is given by

$$\frac{G^{\mathrm{r}}}{G^{\mathrm{s}}} = \frac{|\Gamma(s_k+1+\mathrm{i}\eta)|}{|\Gamma(-s_k+1+\mathrm{i}\eta)|}\frac{\Gamma(-2s_k+1)}{\Gamma(2s_k+1)}\frac{\operatorname{Im}\Lambda^{\mathrm{r}}}{\operatorname{Im}\Lambda^{\mathrm{s}}} \times (2\beta\gamma R')^{2s_k}. \tag{39}$$

The ratio $F^{\mathrm{i}}/G^{\mathrm{i}}$ depends sensitively on the sign of k. We define $\operatorname{sgn} k \equiv k/|k| = \pm 1$, so that

$$\frac{F^{\mathrm{i}}}{G^{\mathrm{i}}} = \left[\frac{\sum_{n=0}^{\infty} b_n}{\sum_{n=0}^{\infty} a_n}\right]^{-\operatorname{sgn} k}, \tag{40}$$

where the summands are given by the recursion relations,

$$\begin{aligned} b_0 &= 1,\\ a_0 &= \frac{2|k|+1}{R'(\gamma \operatorname{sgn} k+1)+\operatorname{sgn} k(3\beta\eta/2)}b_0,\\ a_1 &= \frac{1}{2}[R'(-\gamma\operatorname{sgn} k+1)-\operatorname{sgn} k(3\beta\eta/2)]b_0,\\ b_n &= \frac{[R'(\gamma\operatorname{sgn} k+1)+\operatorname{sgn} k(3\beta\eta/2)]a_n-\operatorname{sgn} k(\beta\eta/2)a_{n-1}}{2|k|+2n+1},\\ a_{n+1} &= \frac{[R'(-\gamma\operatorname{sgn} k+1)-\operatorname{sgn} k(3\beta\eta/2)]b_n+\operatorname{sgn} k(\beta\eta/2)b_{n-1}}{2(n+1)}. \end{aligned} \tag{41}$$

The convergence of Eq. (28) including nuclear size effects has been demonstrated out to $\gamma_{\max} \simeq 10/R'$ [22]. Above this value of the Lorentz factor, evaluation of the confluent hypergeometric function can be problematic. However, even for uranium $\gamma_{\max} \simeq 528$, this is well into the ultrarelativistic limit, which is the topic of Section 2.9.

2.9. The ultrarelativistic limit

Sørensen [23] has shown that for ultrarelativistic ions, a (careful) perturbation treatment of the problem of energy loss is possible. In particular, because of finite nuclear size effects the potential energy experienced by an electron has a maximum depth of order $4Z_1A_1^{-1/3}m_{\mathrm{e}}c^2 \sim 10$ MeV, while the kinetic energies involved are very much greater than this. Thus, the energy loss calculation should be amenable to perturbation methods.

For a uniformly charged nucleus, the perturbation treatment leads to a correction

$$\Delta L_{\mathrm{ultra}} = \frac{1}{2}\int_{-1}^{1}\frac{1-(1-\mu)\beta^2/2}{1-\mu} \times \left[\frac{9}{2(\beta\gamma R')^2}\frac{j_1^2\left(\sqrt{2}\sqrt{1-\mu}\beta\gamma R'\right)}{1-\mu}-1\right]\mathrm{d}\mu. \tag{42}$$

The limiting behavior of this expression is given by

$$\Delta L_{\mathrm{ultra}} = -\ln(\beta\gamma R') - 0.2 + \beta^2/2. \tag{43}$$

The LS correction with the finite nuclear size modification tends toward this same limit. This correction cancels the density effect correction in the ultrarelativistic limit, so that the entire stopping logarithm becomes

$$L = L_0 + \Delta L = \ln\frac{2c}{R\omega_{\mathrm{p}}} - 0.2, \tag{44}$$

where ω_{p} is the plasma frequency of the target material. The physical interpretation is that the impact parameters range from a minimum of order R out to a maximum of order c/ω_{p}. The remarkable simplicity of Eq. (43) allows us to "sweep under the rug" the misbehavior of the confluent hypergeometric function at high Lorentz factor.

The prediction of an energy-independent energy loss in the ultrarelativistic regime has been confirmed with >100 A GeV Pb ions at the CERN-SPS accelerator [24,25]. A comparison of these relativistic effects may be found in Figs. 1 and 2.

2.10. Other ultrarelativistic effects

Although the finite nuclear size effect is the most important modification to energy loss at very high energies, there are a few additional effects which can make a small but significant contribution to slowing.

Ahlen [10] discusses two of these effects and gives approximate formulas. First is a quantum electrodynamical (QED) effect, or radiative correction. The primary physical manifestation of this correction is bremsstrahlung of scattered electrons during electron–projectile collisions. In the derivation of Jankus [26], he gives the correction as an

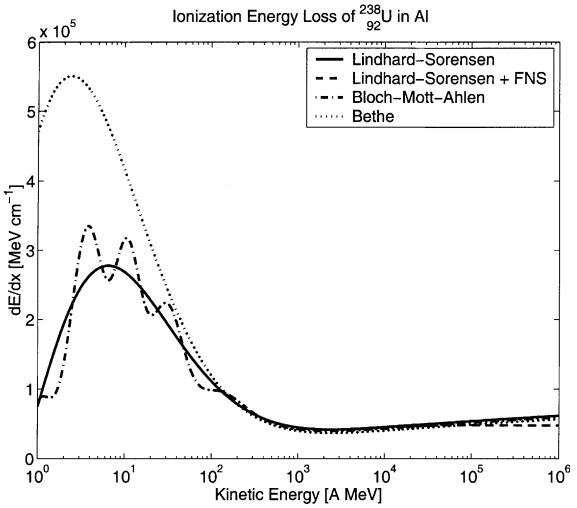

Fig. 1. $\mathrm{d}E/\mathrm{d}x$ as calculated with several important corrections for uranium slowing in aluminum. All computations included the Sternheimer et al. density effect and the HBG electron capture correction.

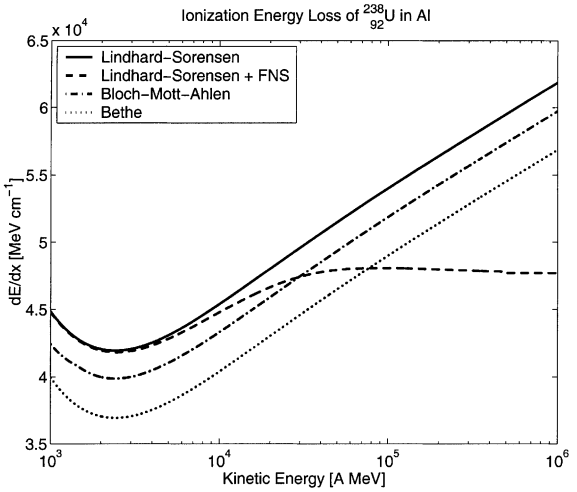

Fig. 2. The high-energy portion of Fig. 1.

entirely separate form of energy loss. In SI units, the energy loss is given by

$$-\frac{\mathrm{d}E_{\mathrm{QED}}}{\mathrm{d}x}=\frac{\alpha Z_1^2 e^4 n_{\mathrm{e}}}{4\pi^2\epsilon_0^2 m_{\mathrm{e}} c^2}L_{\mathrm{QED}}, \tag{45}$$

with the dimensionless factor L_{QED} given by

$$L_{\mathrm{QED}}=\left\{\frac{1}{3}[\ln(2\gamma)]^3+\frac{29}{12}[\ln(2\gamma)]^2 - \left[\frac{217}{36}+\frac{\pi^2}{8}\right]\ln(2\gamma)-\left[\frac{\pi^2}{3}-\frac{7}{4}\right]\ln q + \frac{899}{108}+\frac{\pi^2}{12}-\frac{39}{16}\zeta(3)-\frac{1}{4}\sum_{k=1}^{\infty}\frac{1}{2^k k^3}\right\}. \tag{46}$$

The parameter q, which is a momentum integral cut-off in units of the electron mass, may take on the values $1<q<2\gamma$, but values of q in this range make only a small change in the value of Eq. (45). The sum in the last term has the value $\sum 1/2^k k^3 = 0.5372132\ldots$. Combining Eq. (45) with Eq. (1) we find

$$\Delta L_{\mathrm{QED}}=\frac{\alpha\beta^2}{\pi}L_{\mathrm{QED}}. \tag{47}$$

The other small ultrarelativistic effect is the kinematic correction. This accounts for the finite mass of the nucleus in electron–projectile collisions. We take the projectile mass to be $M_1 = A_1 m_{\mathrm{u}}$, where $m_{\mathrm{u}} = 931.4943\ \mathrm{MeV}/c^2$. This correction has the form

$$\Delta L_{\mathrm{kin}}=-\frac{1}{2}\ln\left(1+2\frac{\gamma m_{\mathrm{e}}}{A_1 m_{\mathrm{u}}}\right)-\frac{1}{2}\frac{m_{\mathrm{e}}}{A_1 m_{\mathrm{u}}}\frac{\beta^2}{\gamma}. \tag{48}$$

We can expect the finite mass correction to become important when the energy of electrons in the rest frame of the projectile is comparable to the mass of the projectile. If we set $\gamma m_{\mathrm{e}} = A_1 m_{\mathrm{u}}$, then $\gamma = 1823 A_1$. This corresponds to approximately 400 A TeV for uranium! At such high energies, other electromagnetic effects are much more important as we will see in Section 2.11. Furthermore, the kinematic effect may actually be damped by finite nuclear size effects. As pointed out by Lindhard and Sørensen [2], the momentum transfer in an electron–nucleus collision should have a maximum of roughly $\hbar/R$. Starting from the initial rest frame of the projectile, after the encounter, the recoil velocity of the projectile will be of order $v_{\mathrm{nuc}}/c \simeq 0.18 A^{-4/3}$. For uranium this is $v_{\mathrm{nuc}}/c \approx 10^{-4}$. Thus we can expect recoil effects to be entirely negligible for nuclei heavier than hydrogen.

2.11. Projectile bremsstrahlung

There are a few ways in which a projectile can lose energy electromagnetically besides Coulomb collisions with electrons. The most important of these are projectile bremsstrahlung and pair production. Projectile bremsstrahlung is distinct from the QED electron bremsstrahlung correction. Here the bremsstrahlung is emitted directly from the projectile in the effective field of the target nuclei. Some of the details of the quantum theory of bremsstrahlung may be found in Heitler [27].

Following Heitler, then, the energy loss due to bremsstrahlung can be placed in the form (in units of A MeV g^{-1} cm^2)

$$-\frac{dE_{rad}}{dx} = \alpha N_A m_u c^2 r_e^2 \left(\frac{m_e}{m_u}\right)^2 \frac{Z_1^4}{A_1^2}\frac{Z_2^2}{A_2}\gamma B, \tag{49}$$

where B is a dimensionless factor analogous to L. It is most interesting to note that unlike the Z_1^2/β^2 dependence in atomic collisions, bremsstrahlung scales as $Z_1^4\gamma$. Thus although ion bremsstrahlung is suppressed relative to electron bremsstrahlung by $(m_e/m_u)^2$, bremsstrahlung can become important for very highly charged ions at energies which are not "too" ultrarelativistic (i.e., energies accessible to present-generation heavy ion accelerators such as CERN-SPS and RHIC).

The explanation of the Z_1^4 dependence is very straightforward. Classically the power radiated by an accelerated particle with charge q is proportional to $q^2|\mathbf{a}|^2$. The acceleration is simply due to the Coulomb force, so $|\mathbf{a}|$ is proportional to q. Altogether power scales like q^4. There is an exact quantum mechanical correspondence. In terms of matrix elements, one must multiply the coupling of the ion to the electromagnetic radiation field ($\sim Z_1$) by the coupling of the ion to the Coulomb field of the target nucleus ($\sim Z_1 Z_2$). Then we square the matrix element to obtain rates and cross-sections, so altogether we have $Z_1^4 Z_2^2$.

The dimensionless factor B is given by

$$B = \left[\frac{12\gamma^2+4}{3\beta\gamma^2} - \frac{6\beta+8}{3\beta^2\gamma^2}\ln(\gamma+\beta\gamma)\right]\ln(\gamma+\beta\gamma) - \frac{4}{3} + \frac{2}{\beta\gamma^2}F_b\big(2\beta\gamma^2(1+\beta)\big), \tag{50}$$

where the "bremsstrahlung function", F_b, is defined by

$$F_b(x) = \int_0^x \frac{\ln(1+y)}{y}\,dy. \tag{51}$$

This integral may be represented by the sum

$$F_b(x) = -\sum_{n=1}^{\infty}\frac{(-x)^n}{n^2}, \tag{52}$$

for $x < 1$. For $x > 1$ the identity

$$F_b(x) = \frac{\pi^2}{6} + \frac{1}{2}(\ln x)^2 - F_b\left(\frac{1}{x}\right) \tag{53}$$

may be used.

There are a few corrections to this formula which Heitler discusses. The first is the correction due to bremsstrahlung off of atomic electrons. This may be included by making the replacement $Z_2^2 \to Z_2(Z_2 + C)$ where $C \approx 0.75$. Another correction is due to the use of the first Born approximation in deriving Eq. (49). A correction of the form

$$\Delta B_{Born} = -4.828(\alpha Z_2)^2 \tag{54}$$

accounts for the inadequacy of the first Born approximation for large Z_2. We may also expect further substantial corrections due to finite nuclear size effects, but this takes us beyond the scope of the present work.

Pair production, sometimes called "sparking the vacuum" is basically a small correction to projectile bremsstrahlung. Ahlen [10] gives the ratio of pair production loss to bremsstrahlung loss,

$$\frac{dE_{pair}}{dE_{rad}} \simeq \frac{A_1}{1000 Z_1^2}\frac{m_u}{m_e}, \tag{55}$$

for ultrarelativistic nuclei.

2.12. Electron capture

With the possible exception of certain low-energy corrections, the influence of electron capture may be the least well understood correction to energy loss. It may not be possible to formulate the influence of electron capture as an additive correction. Intuitively, however, we can imagine that

electron capture may be made manifest as a decrease in the projectile charge: the bare nuclear charge Z_0 is replaced by the effective projectile charge Z_1 in all expressions containing the projectile charge. For energies significantly in excess of 1 A GeV, the effective charge will be very nearly equal to the bare charge. For lower energies, the empirical formula of Pierce and Blann [28] is available,

$$Z_1 = Z_0\left[1 - \exp\left(-\frac{0.95\beta}{\alpha Z_0^{2/3}}\right)\right]. \tag{56}$$

The power $Z_0^{2/3}$ in the exponential is derived from Thomas–Fermi calculations on the target atoms [29,30]. It has been shown experimentally that Z_1 depends on the target material [31]. Anthony and Landford derive the empirical formula [31],

$$Z_1 = Z_0\left[1 - A(Z_2)\exp\left(-\frac{B(Z_2)\beta}{\alpha Z_0^{2/3}}\right)\right], \tag{57}$$

with the functions A and B given by

$$\begin{aligned} A &= 1.16 - 1.91\times 10^{-3}Z_2 + 1.26\times 10^{-5}Z_2^2,\\ B &= 1.18 - 7.5\times 10^{-3}Z_2 + 4.53\times 10^{-5}Z_2^2. \end{aligned} \tag{58}$$

Note that both Eqs. (56) and (57) depend only on projectile velocity, not projectile energy. Thus, these forms for the effective charge will approach a constant value at high energies. For large charges, the resulting difference $Z_0 - Z_1$ may be non-negligible.

More recently, using a fit to a large dataset of energy loss and range data, Hubert et al. [32,33], have proposed the formula

$$Z_1 = Z_0[1 - x_1\exp(-x_2E^{x_3}Z_0^{-x_4})], \tag{59}$$

where E is the kinetic energy in A MeV, and the x parameters are given as follows:

$$\begin{aligned} x_1 &= D + B\exp(-CZ_0),\\ D &= 1.164 + 0.2319\exp(-0.004302Z_2),\\ B &= 1.658,\\ C &= 0.05170,\\ x_2 &= 8.144 + 0.09876\ln Z_2,\\ x_3 &= 0.3140 + 0.01072\ln Z_2,\\ x_4 &= 0.5218 + 0.02521\ln Z_2, \end{aligned}$$

Table 1
Effective charge parameters for the HBG formula for beryllium and carbon

Target	D	B	C	x_2	x_3	x_4
Be	2.045	2.000	0.04369	7.000	0.2643	0.4171
C	2.584	1.910	0.03958	6.933	0.2433	0.3969

where these parameters should be considered valid for all targets except beryllium and carbon which are given in Table 1. A comparison of the effective charge in all three models described here is given in Fig. 3.

2.13. The Barkas correction

The Barkas effect was first noticed as a difference in energy loss between positive and negative pions [34,35], indicating that the energy loss contained odd powers of Z_1. The independent analyses of Ashley et al. [36–38] and Jackson and McCarthy [39] concluded that target polarization effects for low-energy distant collisions would produce a multiplicative correction to the energy loss, that is

$$\frac{dE}{dx} \to \frac{dE_{\text{Barkas}}}{dx} = \frac{dE}{dx}\left(1 + \frac{Z_1}{\sqrt{Z_2}}F(V)\right). \tag{60}$$

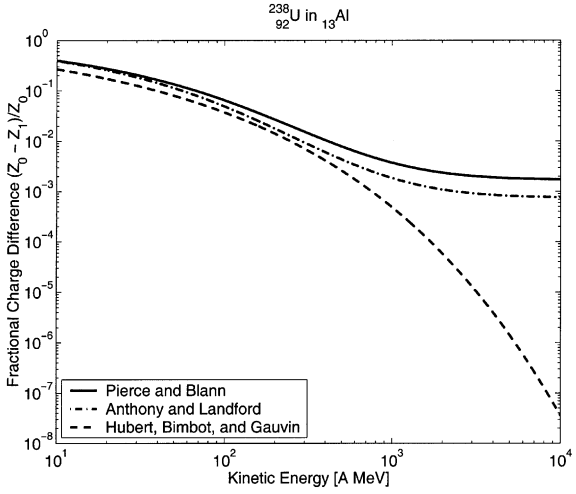

Fig. 3. Effective charge of uranium in aluminum as a function of energy for the different electron capture models described in this work.

Table 2
Values of the Jackson–McCarthy "universal" function

V	$V^2F(V)$	$F(V)$
1.0	0.33	0.33
2.0	0.31	0.078
3.0	0.27	0.03
4.0	0.23	0.014
5.0	0.21	0.0084
6.0	0.19	0.0053
7.0	0.17	0.0035
8.0	0.16	0.0025
9.0	0.15	0.0019
10.0	0.14	0.0014

The variable V is a reduced momentum defined by

$$V = \frac{\beta\gamma}{\alpha\sqrt{Z_2}}. \tag{61}$$

The "universal" function $F(V)$ is a ratio of two integrals over a Thomas–Fermi model of the atom. A figure showing values of $V^2F(V)$ is given in [39]. Also, values of $V^2F(V)$ may be found in Table 2. Jackson and McCarthy do not consider their calculations to be reliable for $V < 0.8$. Interestingly, their calculation also found the close-collision correction to be nearly the same as the first term of the Mott correction (the term proportional to $\eta\beta^2$).

The Barkas effect was actually given its name several years after the Jackson and McCarthy article by Lindhard, who showed [40] that the correction factor should be multiplied by 2 (i.e. $F(V) \to 2F(V)$) to give better agreement with both theoretical results and experimental data. Basically, Jackson and McCarthy should have included close collisions even in the low-energy regime. This was confirmed with a more detailed calculation by Morgan and Sung [41]. Because of the way the Barkas correction is formulated, it has been questioned [42] whether the effect can be deconvolved from the effects of electron capture (i.e. the effective charge Z_1).

2.14. The shell corrections

Shell corrections arise when the velocity of the projectile is comparable to velocities of electrons in target atoms. Two regimes are possible: first, the velocity of the projectile may be low enough so that inner (K, L) shell electrons have velocities comparable to the projectile; second, the inner shell electrons may actually have relativistic velocities for sufficiently heavy target atoms.

For the first type of shell correction, Fano [43] proposed a correction of the form

$$\Delta L_{\text{shell}} = -C/Z_2, \tag{62}$$

where C is a complicated function of the various parameters. Fano also showed that ΔL_{shell} does not vanish at high energies, as was assumed when shell corrections were first discussed. This fact led to widespread use of the "adjusted" shell correction, which is defined by

$$\ln I + C/Z_2 \equiv \ln I_{\text{adj}} + C_{\text{adj}}/Z_2, \tag{63}$$

demanding $\lim_{\beta\to 1} C_{\text{adj}}/Z_2 = 0$. Theoretical calculations of C exist [43–45], as well as some experimental values [46]. In every formulation investigated, C is independent of Z_1. Since most other correction terms we have investigated scale as a positive power of Z_1, it is probably reasonable to assume that the shell correction is not as important as other low-energy corrections, especially the Barkas term. The version of Barkas and Berger [44] is fairly widely accepted,

$$\begin{aligned} C_{\text{adj}} &= (4.22377\times 10^{-7}\beta^{-2}\gamma^{-2} + 3.04043\times 10^{-8}\beta^{-4}\gamma^{-4} \\ &\quad - 3.8106\times 10^{-10}\beta^{-6}\gamma^{-6})I_{\text{adj}}^2 \\ &\quad + (3.858019\times 10^{-9}\beta^{-2}\gamma^{-2} \\ &\quad - 1.667989\times 10^{-10}\beta^{-4}\gamma^{-4} \\ &\quad + 1.57955\times 10^{-12}\beta^{-6}\gamma^{-6})I_{\text{adj}}^3, \end{aligned} \tag{64}$$

where the formula should be considered valid for $\beta\gamma > 0.13$.

The second situation mentioned above was addressed by Leung [47,48] who found an additional relativistic shell correction,

$$\Delta L_{\text{Leung}} = -\frac{5}{3}\ln\left(\frac{2m_e c^2\beta^2}{I}\right)\frac{|B_{\text{tot}}|}{Z_2 m_e c^2} + \frac{I^2}{4m_e^2 c^4\beta^2}, \tag{65}$$

where $B_{\text{tot}} < 0$ is the total ground-state electronic binding energy. Again, it is not clear how this

result scales with projectile charge. In addition we have omitted a term $-\beta^2$ which appears in the correction as defined in [48], since this is probably part of the Bethe form (the derivation is not highly relativistic in the projectile velocity).

3. Comparisons with experiment

We first compared the results of energy loss calculations to experiments already performed. The most useful is the experiment of Ahlen and Tarlé [17], in which a beam of uranium was brought to rest after passing through a series of targets (listed in Table 3). The beam energy was determined to be 955.7 ± 2.0 A MeV by means other than range-energy.

The primary interest of Ahlen and Tarlé was the importance of the BMA group of corrections to dE/dx, so several steps were taken to reduce the importance of additional low-energy corrections. The mean ionization potential I for each target was taken to have its adjusted value I_{adj} (listed in Table 3) as the high-energy limit of the shell correction. The effective projectile charge due to electron capture was computed from the Pierce and Blann formula [28]. Finally all (very uncertain) low-energy corrections were effectively circumvented by using a measured range [49] below 150 A MeV. That is, integrations of dE/dx were carried out only between 150 and 1000 A MeV. Ignoring all corrections in the BMA group, they found a reconstructed beam energy of 903.5 A MeV. Including only the Mott correction the beam energy became 1003.9 A MeV. Clearly, Mott corrections alone are not sufficient for the energy loss of uranium. Finally, they calculated the beam energy including all components of the BMA group with a resulting theoretical energy of 952.8 A MeV, a fractional error of only 0.3%. Although the theoretical uncertainty was not quoted, the uncertainty due to electron capture alone encompasses the measured energy value as they show in their Fig. 2.

As a first test of our own range-energy calculations we sought to reproduce the calculations of Ahlen and Tarlé so that we would have a solid basis against which we could compare other sorts of range-energy calculations. The primary complication is not in the theoretical construction of range-energy code, but in the empirical range used below 150 A MeV. For this we must look to the results of Ahlen et al. [49]. This experiment was also performed at the Bevalac with a beam of 147.7 A MeV uranium. The experimental setup is summarized in Table 4. Note that the range was measured not in Lexan but in CR-39, a somewhat different plastic track-etch detector.

The details of how the conversion of CR-39 range to Lexan range was performed are not described in [17]. There are a variety of ways to perform the range conversion. These include setting the range in Lexan equal to the total range at 147.7 A MeV from [49], setting the range in Lexan equal to the range only in CR-39 (at the appropriate energy) from [49], correcting the range in CR-39 for the different $\langle A_2/Z_2 \rangle$ in Lexan, and correcting the range in CR-39 by the ratio of dE/dx in the two materials. For each technique considered, we computed the beam energy using corrections due to the BMA group or its replacement, the LS correction. The resulting beam energies agreed with the original calculation typically to better than a few tens of A MeV. Furthermore, for each technique the BMA calculation and the LS calculation agreed to typically better than 1 A MeV. Thus, we feel it is

Table 3
Experimental setup in the Ahlen and Tarlé experiment

Target	Thickness (g cm^{-2})	I_{adj} (eV)
Al (beam window)	0.137 ± 0.020	166 ± 1
Air	0.0426 ± 0.0020	85.4 ± 1.0
Cu	8.3162 ± 0.0010	323 ± 2
Lexan	2.327 ± 0.002	67.0 ± 1.0

Table 4
Experimental setup in the Ahlen, Tarlé and Price experiment[a]

Target	Thickness (g cm^{-2})
Al (beam window) + Air	0.2039 ± 0.014
CR-39	0.3771 ± 0.0005
Total range	0.581 ± 0.014

[a] The individual thicknesses of Al beam-pipe window and air were not quoted in the article.

Table 5
Beam energy reconstructions by the method of direct integration

Method	Energy (A MeV)
No Barkas	
Bethe	899.4
BMA	931.9
LS	947.3
With Barkas	
Bethe	908.5
BMA	948.6
LS	957.0
Beam energy	955.7 ± 2.0

quite valid to replace the BMA group with the LS correction.

Because of the uncertainty of the range conversion, we also considered the direct integration of dE/dx. As there is no suggestion of how shell corrections scale with projectile charge, we ignored these entirely. More significant, however, is the Barkas correction which was included for some calculations. Results are summarized in Table 5. The "Bethe" method uses the bare Bethe formula plus the density effect correction. "BMA" is "Bethe" plus the BMA group. "LS" is "Bethe" plus the LS correction (finite nuclear size effects are negligible at this energy and were not included). Each method was performed with and without the Barkas correction.

In 1999 we had the opportunity to repeat Ahlen and Tarlé's experiment. We made use of the 1.0 A GeV uranium beam at the GSI laboratory in Darmstadt, Germany. Table 6 shows the experimental setup in the 1999 GSI exposure. The details of the beam window and wire chamber are from Schardt [50]. In addition, the beam energy was 1000.0 ± 0.5 A MeV with a spread of 0.15% about this central value.

The Lexan target consisted of 103 sheets of Lexan plastic, each about 260 μm in thickness. The range in Lexan was determined by scanning the sheets near the stopping point of the main beam, determined by visual comparison of track density on upstream and downstream sheets. The positions of events found in the scans were matched on adjacent sheets. A steep decline in the number of matches was observed to begin at around 2.7 $g\,cm^{-2}$ and continue to about 2.75 $g\,cm^{-2}$. The midpoint of this decline was taken to be the stopping point for the purpose of calculating energy, with the uncertainty determined by the thickness of one Lexan sheet to either side of the stopping point.

The results of the energy reconstruction are shown in Table 7. The various effects included in the reconstruction are also shown. In both cases, the range was integrated up from 8 A MeV, with the energy at 8 A MeV given by the Benton and Henke [52] range code.

Table 6
Experimental setup in the 1999 GSI exposure

Target	Substance	Thickness ($mg\,cm^{-2}$)	I (eV)
Beam window	Hostaphan ($C_{10}H_{10}O_4$)	22.8	72.3
	Kevlar ($C_{14}H_{14}N_2O_2$)	12.1	71.7
Air	Air	7.23	85.4
Wire chamber	Kapton ($C_{22}H_{10}N_2O_5$)	3.55	75.9
	Mesh	5.16	223.0
	Ar (80%) CO_2 (20%)	19.0	174.7
	Kapton ($C_{22}H_{10}N_2O_5$)	3.55	75.9
Air	Air	32.5	85.4
Copper absorber	Cu	8669.7 ± 4.5	323.0
Lexan target	Lexan ($C_{16}H_{14}O_3$)	2725 ± 32	73.1

Table 7
Results of energy reconstruction from range in the 1999 GSI exposure

Effects included	Energy (A MeV)
LS Electron capture[a] Density effect[b]	1009.0 ± 2.7
LS Electron capture[c] Density effect[b] Shell Effect[d] Leung effect	1002.2 ± 2.7
Beam energy	1000.0 ± 0.5

[a] Version of Hubert et al. [32,33].
[b] Version of Sternheimer et al. [7].
[c] Version of Anthony and Landford [31].
[d] Version of Barkas and Berger [51].

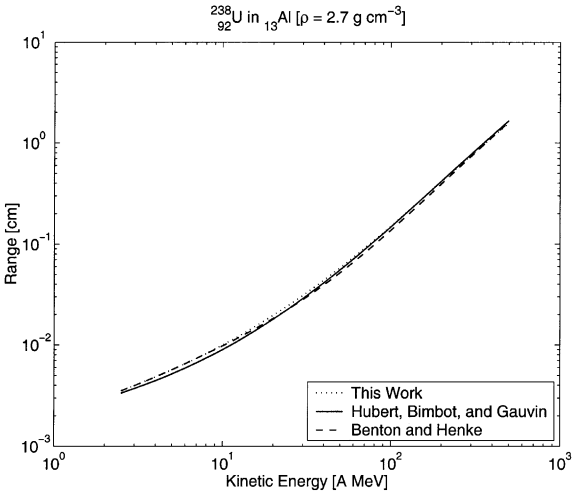

Fig. 4. Comparison of ranges of uranium in aluminum from three different sources.

4. Comparisons with theory

To test the general accuracy of the code developed as part of this study we compared range and energy loss to the code developed by Benton and Henke [52] (hereinafter BH) and to the tables of Hubert, Bimbot and Gauvin (hereinafter HBG). The HBG tables cover the energy regime 2.5–500 A MeV, so the comparison was performed only in this region. Both BH and HBG ranges are based on experimental measurements. In the case of BH, the code is based on parametric fits to the range tables of Barkas and Berger [51]. HBG extrapolated their tables from a large experimental data set. The comparison was performed using the LS correction (without finite nuclear size which is negligible at these energies), the density effect of Sternheimer et al. [7], and HBG's own version of electron capture.

Fig. 4 shows the comparison among all three sources. This log–log plot is only intended to show the overall shape of the curves in this energy region. Fig. 5 shows the fractional differences $(R - R_{\mathrm{BH}})/R_{\mathrm{BH}}$ and $(R - R_{\mathrm{HBG}})/R_{\mathrm{HBG}}$, where R is the range computed with our own code. Since the code developed in this work is based on the BH ranges below 8 A MeV, that fractional difference is extremely small at low energies. Fig. 6 shows a comparison of $\mathrm{d}E/\mathrm{d}x$ computed from the three sources. The BH code contains three different parameterizations covering different energy regions. The dip in the BH value of $\mathrm{d}E/\mathrm{d}x$ at about 7 A MeV is due to a slight imperfection in the joining of two parameterization regions. The join between the different parameterization regions is optimized for continuity in range and $\mathrm{d}E/\mathrm{d}x$, so it is not surprising to see a discontinuity in the value of $\mathrm{d}^2E/\mathrm{d}x^2$.

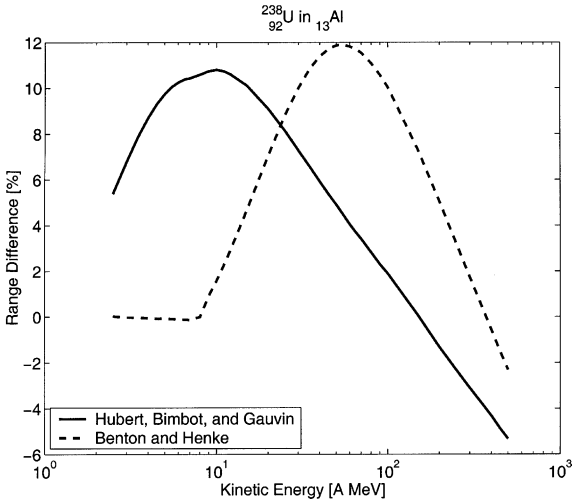

Fig. 5. Fractional differences (in percent) for the range code developed in this work compared to two other sources.

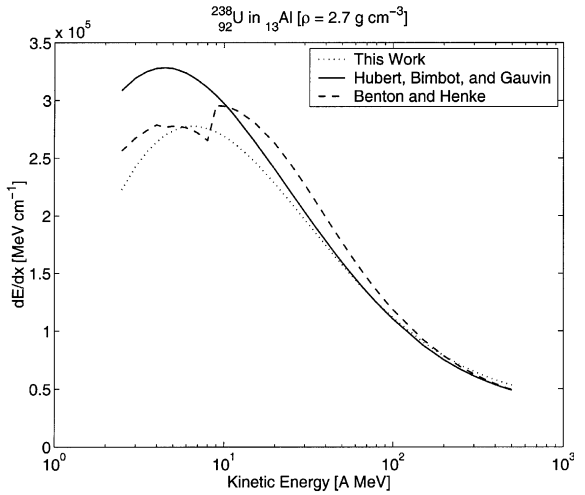

Fig. 6. Comparison of energy loss of uranium in aluminum from three different sources.

5. Conclusion

The code developed as part of this study is certainly accurate enough for applications in cosmic-ray astrophysics and most other purposes. It is accurate to ≈0.2% in the reconstruction of energy as a function of range in actual experiments and agrees to better than 10% with existing codes and tables in the theoretically troublesome low-energy region. Fig. 6 is especially revealing when compared to Fig. 1. Without the LS correction (which reduces to the Bloch correction in the energy region of Fig. 6) there would be a disagreement of roughly a factor of 2 between the code developed in this work and older codes and tabulations. With the exception of electron capture, the LS correction completely dominates all low-energy effects. This is to be expected, since the Bloch correction scales as Z_1^2, the Barkas effect scales as Z_1 and the shell and Leung corrections, which are primarily concerned with the velocity of inner shell electrons of the target atoms, should not be expected to scale as Z_1 at all.

The code developed during this study can be found at http://ultraman.ssl.berkeley.edu/~weaver/dedx/. The code requires the use of a C compiler to run.

Acknowledgements

Many thanks to Hans Bichsel, Jay Cummings, Pui-Tak Leung, Michael Salamon, Christoph Scheidenberger, Steven Seltzer, Allan Sørensen and Greg Tarlé for assistance during the research into energy loss effects. We would like to thank Louis Bernhardt, Dieter Schardt and Reimar Spohr of the Gesellschaft für Schwerionenforschung in Darmstadt, Germany for assistance during uranium beam exposures. We would like to thank Michael Solarz for assistance in etching Lexan.

Appendix A. Gamma function

The complex Gamma function appears frequently in these calculations. In particular, the argument of the Gamma function appears in the Mott correction, the Ahlen correction, and the LS correction. To very high precision the Gamma function is given by [53]

$$\Gamma(z+1) = \left(z+\gamma+\frac{1}{2}\right)^{z+\frac{1}{2}} \exp\left[-\left(z+\gamma+\frac{1}{2}\right)\right] \times \sqrt{2\pi}\left[c_0 + \sum_{k=1}^{N} \frac{c_k}{z+k} + \epsilon\right]. \quad \text{(A.1)}$$

For special choices of γ, N, and the parameters c_k, the error term $|\epsilon| < 2 \times 10^{-10}$ everywhere in the right complex plane, $\mathrm{Re}\, z > 0$. The special choices are $\gamma = 5$, $N = 6$, and

$$\begin{aligned} c_0 &= 1.000000000190015, \\ c_1 &= 76.18009172947146, \\ c_2 &= -86.50532032941677, \\ c_3 &= 24.01409824083091, \\ c_4 &= -1.231739572450155, \\ c_5 &= 0.1208650973866179 \times 10^{-2}, \\ c_6 &= -0.5395239384953 \times 10^{-5}. \end{aligned} \quad \text{(A.2)}$$

With some effort, the real and imaginary parts can be extracted from this formula and from these, the absolute value and the argument. If we let $z = x + \mathrm{i}y$, then we must define two parameters

$$T = -y\sum_{k=1}^{6}\frac{c_k}{(x+k)^2+y^2} \tag{A.3}$$

and

$$B = c_0 + \sum_{k=1}^{6}\frac{c_k(x+k)}{(x+k)^2+y^2}. \tag{A.4}$$

Now we have

$$\ln|\Gamma(z+1)| = \frac{1}{2}\left(x+\frac{1}{2}\right)\ln\left[(x+5.5)^2+y^2\right] - y\arctan\frac{y}{x+5.5} - (x+5.5) + \ln\sqrt{2\pi(T^2+B^2)} \tag{A.5}$$

and

$$\arg\Gamma(z+1) = \frac{y}{2}\ln\left[(x+5.5)^2+y^2\right] + \left(x+\frac{1}{2}\right)\arctan\frac{y}{x+5.5} - y + \arctan\frac{T}{B}. \tag{A.6}$$

For operations taking place in the left complex plane $\mathrm{Re}\, z < 0$, it is handy to know the reflection formula

$$\Gamma(1-z)\Gamma(1+z) = \frac{\pi z}{\sin \pi z}. \tag{A.7}$$

The Gamma function has poles at zero and all negative integers, and that behavior is reproduced faithfully in this formula.

Appendix B. Confluent hypergeometric function

The confluent hypergeometric function, $M(a, b, z)$ (alternatively ${}_1F_1(a, b; z)$) appears in the finite nuclear size correction to the LS correction. The simplest representation is

$$M(a,b,z) = 1 + \frac{\Gamma(b)}{\Gamma(a)}\sum_{n=1}^{\infty}\frac{\Gamma(a+n)}{\Gamma(b+n)}\frac{z^n}{n!}, \tag{B.1}$$

with a, b, z complex numbers. The implementation of this formula would seem to require an excessive number of calls to the Gamma function, but we recognize here the so-called Pochhammer symbol

$$\frac{\Gamma(z+n)}{\Gamma(z)} = z(z+1)(z+2)\cdots(z+n-1) \equiv (z)_n, \tag{B.2}$$

so that Eq. (B.1) becomes

$$M(a,b,z) = 1 + \sum_{n=1}^{\infty}\frac{(a)_n}{(b)_n}\frac{z^n}{n!}. \tag{B.3}$$

Each term in the series can be obtained from the previous one by multiplying by $(a+n-1)z/(b+n-1)n$ and thus requires only complex multiplication. Further properties of the confluent hypergeometric function may be found in [54].

References

[1] J.D. Jackson, Classical Electrodynamics, second ed., John Wiley, New York, 1975.
[2] J. Lindhard, A.H. Sørensen, Relativistic theory of stopping for heavy ions, Phys. Rev. A 53 (1996) 2443.
[3] W.H. Bragg, R. Kleeman, On the α particles of radium, and their loss of range in passing through various atoms and molecules, Philos. Mag. 10 (1905) 318.
[4] M.J. Berger et al., Stopping powers for electrons and positrons, in: ICRU Reports, Vol. 37, International Commission on Radiation Units and Measurements, Bethesda, Maryland, 1984.
[5] E. Fermi, The ionization loss of energy in gases and in condensed materials, Phys. Rev. 57 (1940) 485.
[6] R.M. Sternheimer, R.F. Peierls, General expression for the density effect for the ionization loss of charged particles, Phys. Rev. B 3 (1971) 3681.
[7] R.M. Sternheimer, M.J. Berger, S.M. Seltzer, Density effect for the ionization loss of charged particles in various substances, Atom. Dat. Nucl. Dat. Tab. 30 (1984) 261.
[8] S.M. Seltzer, 2000, Private communication.
[9] F. Bloch, Zur Bremsung rasch bewegter Teilchen beim Durchgang durch Materie, Ann. Phys. (Leipzig) 16 (1933) 285.
[10] S.P. Ahlen, Theoretical and experimental aspects of the energy loss of relativistic heavily ionizing particles, Rev. Mod. Phys. 52 (1980) 121.
[11] G. Tarlé, M. Solarz, Evidence for higher-order contributions to the stopping power of relativistic iron nuclei, Phys. Rev. Lett. 41 (1978) 483.
[12] M.H. Salamon, S.P. Ahlen, G. Tarlé, K.C. Crebbin, Measurement of higher-order corrections to stopping power for relativistic Ne, Ar, and Fe beams, Phys. Rev. A 23 (1981) 73.
[13] S.P. Ahlen, Z_1^7 stopping-power formula for fast heavy ions, Phys. Rev. A 17 (1978) 1236.
[14] J.A. Doggett, L.V. Spencer, Elastic scattering of electrons and positrons by point nuclei, Phys. Rev. 103 (1956) 1597.

[15] R.M. Curr, The Coulomb scattering of high-energy electrons and positrons by nuclei, Proc. Phys. Soc. (London) 68 (1955) 156.
[16] S.P. Ahlen, Calculation of the relativistic Bloch correction to stopping power, Phys. Rev. A 25 (1982) 1856.
[17] S.P. Ahlen, G. Tarlé, Observation of large deviations from the Bethe–Bloch formula for relativistic uranium ions, Phys. Rev. Lett. 50 (1983) 1110.
[18] C.J. Waddington, P.S. Freier, D.J. Fixsen, Stopping of 200-GeV gold nuclei in nuclear emulsions, Phys. Rev. A 28 (1983) 464.
[19] P. Sigmund, Stopping power in perspective, Nucl. Instr. and Meth. B 135 (1998) 1.
[20] M.E. Rose, Relativistic Electron Theory, Wiley, New York, 1961.
[21] C.P. Bhalla, M.E. Rose, Finite nuclear size effects in β decay, Phys. Rev. 128 (1962) 774.
[22] A.H. Sørensen, 1999, Private communication.
[23] A.H. Sørensen, Electron-ion momentum transfer at ultra-relativistic energy, in: F. Aumayr, H. Winter (Eds.), Photonic, Electronic and Atomic Collisions; Twentieth International Conference on the Physics of Electronic and Atomic Collisions, World Scientific, Singapore, 1998, p. 475.
[24] C. Scheidenberger, Untersuchung der Abbremsung relativistischer Schwerionen in Materie im Energiebereich (100–1000) MeV/u, Ph.D. Thesis, Universität Gießen, 1994.
[25] S. Datz, H.F. Krause, C.R. Vane, H. Knudsen, P. Grafström, R.H. Schuch, Effect of nuclear size on the stopping power of ultrarelativistic heavy ions, Phys. Rev. Lett. 77 (1996) 2925.
[26] V.Z. Jankus, Radiative correction for the collision loss of heavy particles, Phys. Rev. 90 (1953) 4.
[27] W. Heitler, The Quantum Theory of Radiation, third ed., Oxford University Press, London, 1954.
[28] T.E. Pierce, M. Blann, Stopping powers and ranges of 5–90-MeV S^{32}, Cl^{35}, Br^{79}, and I^{127} ions in H_2, He, N_2, Ar, and Kr: A semiempirical stopping power theory for heavy ions in gases and solids, Phys. Rev. 173 (1968) 390.
[29] N. Bohr, The penetration of atomic particles through matter, Kgl. Danske Videnskab. Selskab., Mat.-Fys. Medd. 18 (8) (1948) 1.
[30] N. Bohr, J. Lindhard, Electron capture and loss by heavy ions penetrating through matter, Kgl. Danske Videnskab. Selskab., Mat.-Fys. Medd. 28 (7) (1954) 1.
[31] J.M. Anthony, W.A. Landford, Stopping power and effective charge of heavy ions in solids, Phys. Rev. A 25 (1982) 1868.
[32] F. Hubert, R. Bimbot, H. Gauvin, Semi-empirical formulae for heavy ion stopping powers in solids in the intermediate energy range, Nucl. Instr. and Meth. B 36 (1989) 357.
[33] F. Hubert, R. Bimbot, H. Gauvin, Range and stopping-power tables for 2.5–500 MeV/nucleon heavy ions in solids, Atom. Dat. Nucl. Dat. Tab. 46 (1990) 1.
[34] W.H. Barkas, N.J. Dyer, H.H. Heckmann, Resolution of the Σ^--mass anomaly, Phys. Rev. Lett. 11 (1963) 26.
[35] H.H. Heckman, P.J. Lindstrom, Stopping-power differences between positive and negative pions at low velocities, Phys. Rev. Lett. 22 (1969) 871.
[36] J.C. Ashley, R.H. Ritchie, W. Brandt, Z_1^3 effect in the stopping power of matter for charged particles, Phys. Rev. B 5 (1972) 2393.
[37] J.C. Ashley, R.H. Ritchie, W. Brandt, Z_1^3-dependent stopping power and range contributions, Phys. Rev. A 8 (1973) 2402.
[38] J.C. Ashley, R.H. Ritchie, W. Brandt, Z_1^3-dependent range contributions, Phys. Rev. A 10 (1974) 737.
[39] J.D. Jackson, R.L. McCarthy, Z^3 corrections to energy loss and range, Phys. Rev. B 6 (1972) 4131.
[40] J. Lindhard, The Barkas effect—or Z_1^3, Z_1^4 corrections to stopping of swift charged particles, Nucl. Instr. and Meth. 132 (1976) 1.
[41] S.H. Morgan Jr., C.C. Sung, Z_1^3 contribution to the energy loss of heavy charged particles, Phys. Rev. A 20 (1979) 818.
[42] C.J. Waddington, D.J. Fixsen, H.J. Crawford, P.J. Lindstrom, H.H. Heckman, Stopping of relativistic heavy ions in various media, Phys. Rev. A 34 (1986) 3700.
[43] U. Fano, Penetration of protons alpha particles and mesons, Ann. Rev. Nucl. Sci. 13 (1963) 1.
[44] H. Bichsel, Passage of charged particles through matter, in: D.E. Gray (Ed.), AIP Handbook, third ed., McGraw-Hill, New York, 1972, Chapter 8, p. 142.
[45] H. Bichsel, Stopping power and ranges of fast ions in heavy elements, Phys. Rev. A 46 (1992) 5761.
[46] H.H. Andersen, J.F. Bak, H. Knudsen, B.R. Nielsen, Stopping power of Al, Cu, Ag, and Au for MeV hydrogen, helium, and lithium ions. Z_1^3 and Z_1^4 proportional deviations from the Bethe formula, Phys. Rev. A 16 (1977) 1929.
[47] P.T. Leung, Bethe stopping-power theory for heavy-target atoms, Phys. Rev. A 40 (1989) 5417.
[48] P.T. Leung, Addendum: Bethe stopping-power theory for heavy-target atoms, Phys. Rev. A 60 (1999) 2562.
[49] S.P. Ahlen, G. Tarlé, P.B. Price, Studies of relativistic uranium nuclei with dielectric track detectors, Science 217 (1982) 1139.
[50] D. Schardt, 1999, Private communication.
[51] W.H. Barkas, M.J. Berger, Tables of energy losses and ranges of heavy charged particles, in: U. Fano (Ed.), Studies in Penetration of Charged Particles in Matter, Nuclear Science Series, Vol. 39, National Academy of Sciences—National Research Council, Washington, DC, 1964, Chapter 7, p. 103, publication 1133.
[52] E.V. Benton, R.P. Henke, Heavy particle range-energy relations for dielectric nuclear track detectors, Nucl. Instr. and Meth. 67 (1969) 87.
[53] W.H. Press, S.A. Teukolsky, W.T. Vetterling, B.P. Flannery, Numerical Recipes in C, second ed., Cambridge University Press, Cambridge, 1992.
[54] L.J. Slater, Confluent hypergeometric functions, in: M. Abramowitz, I.A. Stegun (Eds.), Handbook of Mathematical Functions, Applied Mathematics Series, Vol. 55, National Bureau of Standards, Washington, DC, 1964, p. 503.